HOT SPOTS IN TURBOEXPANDER BEARINGS: CASE HISTORY, STABILITY ANALYSIS, MEASUREMENTS AND OPERATIONAL EXPERIENCE

Joachim Schmied
DELTA JS, Switzerland

Josef Pozivil
Cryostar SAS, France

Joseph Walch
Cryostar SAS, France

ABSTRACT

Vibration induced hot spots in radial fluid film bearings can cause spiral vibrations. The phenomenon is known as Morton effect. Various authors have described the phenomenon of spiral vibrations caused by rubbing in general [1 - 4] and specifically by the differential viscous shearing in fluid film bearings [5 - 8]. The history of the case of a turbo-expander for the cryogenic industry is described. The investigated machine has a single relatively stiff rotor with two overhung impellers. The rotor is supported on two tilting pad bearings, as they are commonly used for these applications. It was designed in line with API 617 7th edition [11]. During internal factory testing excessive vibration at high speed suddenly developed, in spite of very high damping and comfortable separation margins of the relevant rotor vibration modes. The vibrations evolution in a polar plot had the appearance of a spiral, as they are typically observed in case of vibration induced hot spots. The tilting pad bearings were suspected as the most likely cause for the hot spots. In parallel to the tests, hot spot stability analyses with a rotor dynamic model of the turbo-expander were carried out. The applied method, introduced by Schmied [5] allows the handling of general rotor systems. The hot spot model is based on the theory of Kellenberger [3] using a thermal equation between the shaft's thermal deflection and the shaft displacement at the hot spot location. The analytical results gave evidence of the instabilities and confirmed the fluid-film bearings as the source of the hot spot. The model was used to assess changes for the solution of the problem. The following measures were studied: Reduction of the oil viscosity, stiffening of the rotor and reduction of the bearing width. The final successfully implemented solution was a combination of lower bearing width and reduced viscosity. Apart from this thoroughly studied case, an overview of further turbo-expanders regarding their hot spot behavior is given.

INTRODUCTION

Hot spot induced spiral vibrations are observed in various types of rotating machinery, e.g. compressors, water turbines, steam turbines and turbo-generators. The hot spots are typically generated by friction due to soft rubbing of the shaft to stationary (non-rotating) parts. Such parts can be labyrinth seals, seal rings, brushes and slip rings in electric machines and even oil lubricated bearings. The hot spot on the shaft surface arises if the rubbing is caused by a synchronous vibration. Since the hot spot thermally bents the shaft and thus changes the synchronous vibration, it moves on the shaft surface, thus causing a phase angle and amplitude change of the synchronous vibration in a polar plot. The vibration signal in the polar plot then has the appearance of a spiral.

Although the phenomenon is known for as long as more than 80 years [1], it has taken quite a while until it became clear, that the phenomenon can also be caused in oil lubricated bearings. In 1987, it was suspected and some theoretical evidence was given, but the hot spot in the bearing was not measured [5]. The phenomenon in the bearing was clearly experimentally verified by temperature measurements on the rotor only in 1996 [6]. Further researchers then contributed to the understanding of the phenomenon [7, 8].

In [6], the phenomenon was observed in a compressor with a large overhung coupling mass causing a typical overhang vibration mode. Other machines prone to the phenomenon due to such vibration modes are gear compressor pinions, which have overhung impeller masses. Several problems due to hot spots with this type of machine are described in [9]. In the conclusion of this paper, which is written by a rotating equipment specialist , who has experience with many compressor vendors, it says: "There is solid evidence, that bearing effects can cause thermal spiral vibration, even with tilting pad bearings." Gear compressor pinions additionally have the effect of a load dependence of the rotor dynamic behavior due to the varying mesh force causing different bearing loads.

CASE HISTORY

Cryogenic expansion turbines are used in air separation plants, in the natural gas processing industry, for energy recovery in pressure let down stations as well as in organic Rankine or Kalina cycles.

The dual expansion turbine/booster compressor loaded unit as shown in Fig. 1 is used to provide refrigeration for the tail gas purification/treatment process in an ethylene processing plant. The two turbines and the two compressor stages are operating in series.

Figure 1. Dual turboexpander 2-TC 400/90 with the oil unit and control panel assembled in the workshop

The turbo-expanders in this case are very robust stiff shaft machines of proven design, for operation up to rather high maximum continuous operating speed (MCOS) of 18'600 rpm. At this MCOS speed the journal bearing peripheral velocity is about 88 m/s.

During the internal testing of the turbo-expanders, the measured shaft vibration started to rise suddenly just above the nominal speed. The sudden vibration increase was identified as a spiral vibration as described in [5]. The bearings were considered as the most likely source for a hot spot. Hot spot stability analyses were performed to confirm these test findings, and different remedies were considered for the machines based on these analyses. Two described remedies as described below were implemented and extensively tested at speeds up to 22'000 rpm (bearing journal velocity 104 m/s), a speed which is much higher than the machine trip speed of 19'500 rpm.

After the successful internal testing the machines were given free for factory acceptance test (FAT) witnessed by customer. The performance and mechanical behavior of both machines were accepted by the customer without reservations.

DESCRIPTION OF THE MACHINE

The expansion turbine is of the radial inflow type with advanced aerodynamic design maximizing the isentropic efficiency. The machine is of a cartridge concept, which allows a quick replacement of the machinery bearing carrier including the rotating parts without interference with the expander cold insulated process pipes.

Adjustable nozzles are located around the expander wheel to control the gas flow by changing the flow area.

A 3D backwards lean blades compressor wheel is employed as a loading device, to recover the mechanical energy from the expander.

A vane diffuser is provided at the compressor wheel periphery to optimize the booster head-flow characteristics and to maximize its efficiency.

The stiff shaft is supported in the bearing carrier by two tilting pad bearings with multi lobe axial face for the thrust load. The radial bearings have 5 pads. They are loaded by the rotor weight of about 120 kg, which yields a specific bearing load of about 0.24 N/mm^2. The load direction is on pad.

The bearing support structure is relatively stiff compared to the oil film and can therefore be regarded as rigid.

The bearing carrier also includes the labyrinth seals and supports the expander nozzle assembly and booster diffuser. The wheels are connected to the shaft by a Hirth radial spur tooth coupling and tightening bolt. The assembly of the bearing carrier with nozzle assembly, diffuser and shrouds is called plug-in unit. Expander and compressor housings are assembled on each side of the flanged bearing carrier (see Fig. 2).

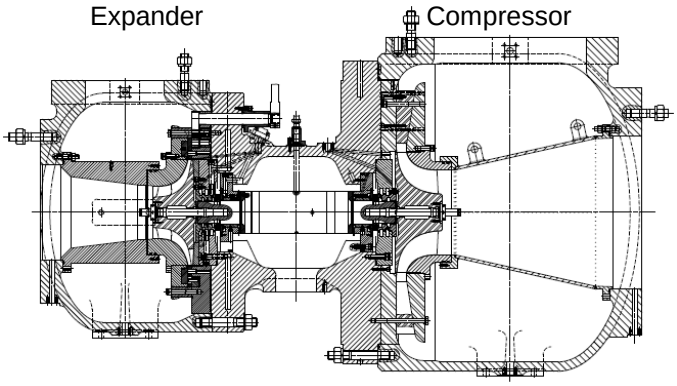

Figure 2. Cross section of the turboexpander TC 400/90

ROTOR DYNAMIC BEHAVIOR (ANALYSIS AND TEST)

Calculated basic rotor dynamic behavior

The Campbell diagram (natural frequencies and damping ratios as a function of speed) of the shaft is shown in Fig. 3 together with the mode shapes of the forward whirling modes. The speed range from the nominal speed to maximum continuous speed in the diagram is grey shaded. There are two forward and backward whirling rigid body modes below nominal speed with a very high damping (damping ratio >20%). The forward whirling 1st and 2nd bending modes are above the speed range with a comfortable separation margin. The backward whirling 1st bending mode coincides with the speed at the maximum continuous speed. However, it cannot be excited by unbalance or thermal bending.

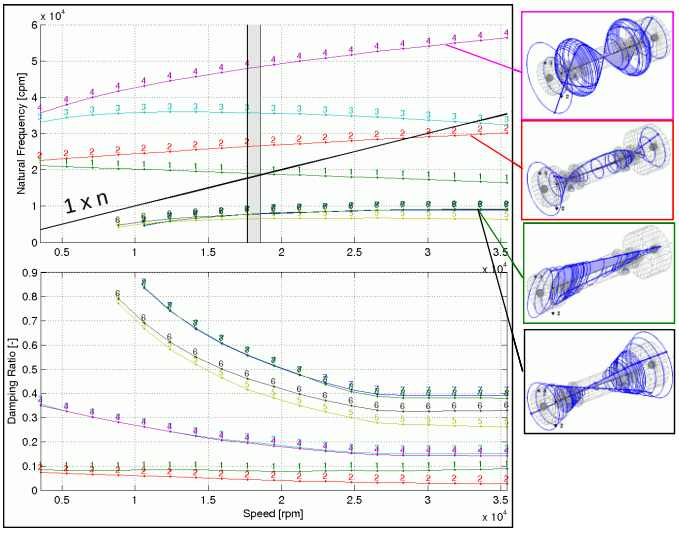

Figure 3. Campbell diagram and mode shapes

Although the shaft has two large overhung masses there are no typical overhang modes thanks to the stiff design. The 1st bending mode has its largest deflection at the impellers; however, the vibration node is outside the bearing.

The response to an unbalance with a magnitude of 4 times the API residual unbalance (165gmm) [11] is shown in Fig. 4. The unbalance distribution as indicated in the figure excites the 1st bending mode. The unbalance magnitude is based on the complete rotor weight, not just on the overhung portions as for overhang modes. The evaluation of the response according to API is also shown in the figure. It can be seen, that the separation margin (SM) of 55.5% is by far larger than the required margin of 25.6%, which depends on the amplification factor (AF) and damping, respectively. The unbalance sensitivity of 0.437 (amplitude limit A_l / amplitude in the critical A_c) is smaller than the required 0.5, although it is not an issue because of the large separation margin. The API evaluation is automatically done in the program MADYN 2000 [10], which has been used for the analysis of the basic behavior.

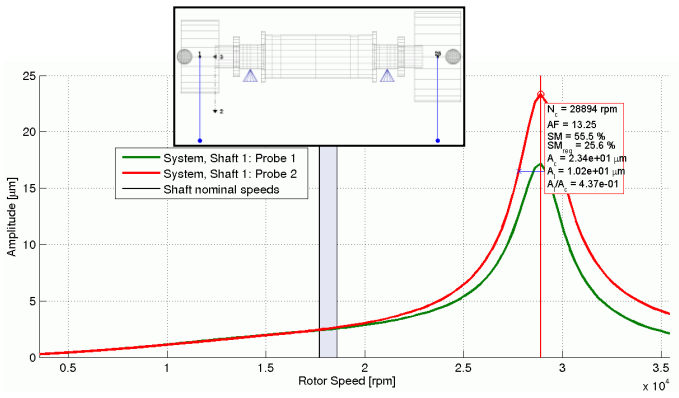

Figure 4. Unbalance response plot with API evaluation

Test bed measurements of original configuration

During the internal performance test of the machines also the mechanical machine behavior was tested up to the trip speed of 19'500 rpm, following the API 617 test requirements [11]. The vibrations were monitored utilizing the Bently Nevada ADRE system. Figure 5 shows the typical test bed computer mimic for the automated performance data monitoring and acquisition.

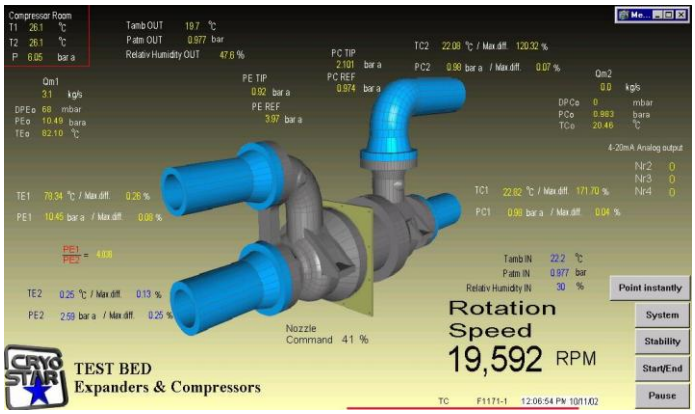

Figure 5. Test bed computer mimic

The measured vibration of the tested machine had a dominant synchronous (1xN) component. The ADRE vibration polar plot (all plots show only this 1xN component) had the typical spiral vibration appearance, as shown in Fig. 6 for the MCOS speed of 18'600 rpm. The rotation direction of the spiral vibration was forward (co-rotational). The time period for 360° phase angle change was around 5 minutes.

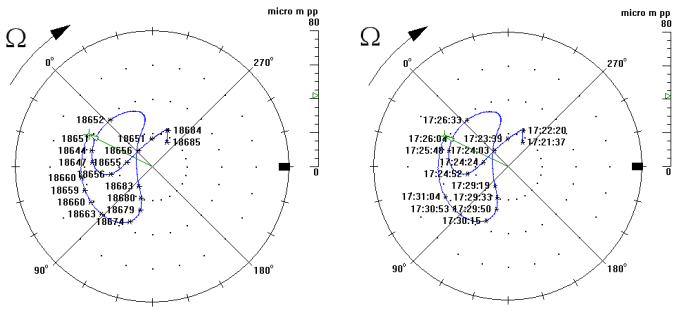

Figure 6a. Spiral vibration in polar plot – expander side

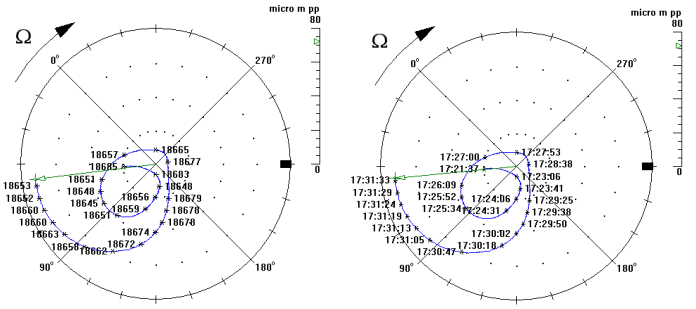

Figure 6b. Spiral vibration in polar plot – compressor side

A hysteresis between run up and run down can be seen in the vibration versus speed plot (Bode plot), Fig. 7. It is a typical behavior for a spiral vibration.

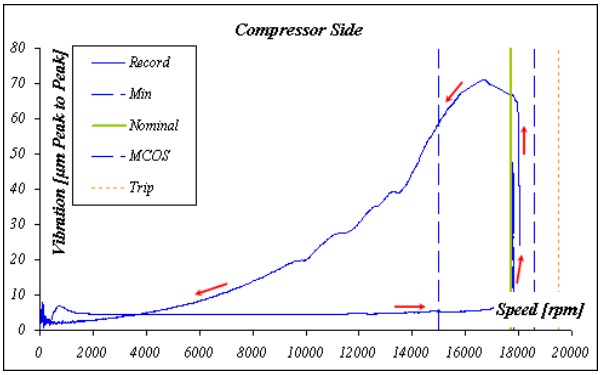

Figure 7. Vibration hysteresis in Bode plot

Several additional internal mechanical running tests were performed with higher and lower oil temperature, with higher and lower oil pressure and thus flow and also with increased and decreased radial bearing clearance. Some of these tests brought little improvements in the shaft vibration behavior, but did not eliminate the hot spot phenomena and the spiral vibration. Therefore it was decided to perform extensive theoretical hot spot stability analyses prior to envisage rotor and bearings modifications.

HOT SPOT STABILITY ANALYSIS

The method introduced by Schmied [5] to calculate the hot spot stability based on the hot spot model of Kellenberger [3,4] is described in detail in appendix A. The method can be used for any rotor system and heating mechanism (also see [12]). Several heating locations can be considered in one model at once. The stability threshold is calculated as a function of the ratio of added to eliminated heat. The added heat is assumed to be proportional to the speed and shaft deflection at the hot spot location, the eliminated heat proportional to the thermal deflection. Thus the stability threshold is a function of the ratio $p\Omega/q$ with p as the proportionality factor for the added heat, q for the eliminated heat and Ω as the speed.

The proportionality factors depend on the heating mechanism and must be derived accordingly. The heating mechanism in a bearing is briefly described in the following paragraph. The corresponding proportionality factors can be estimated with some simplifications as described in appendix B.

If the ratio of added to eliminated heat is close to the threshold or even above the threshold, the rotor can be regarded as sensitive to bearing hot spots.

Hot spot mechanism in the bearing

In Fig.8 the shaft is shown in the bearing for a centered, circular orbit in two positions denoted as 1 and 2 together with the velocity profile of the oil film. Position 2 is a quarter period later than position 1. It is obvious, that for each position, there is one point on the shaft surface, which is subject to maximum friction due to the maximum velocity gradient (red profile). The opposite point of the shaft is subject to the minimum friction due to the minimum gradient (blue profile). In case of a synchronous orbit it is always the same point on the shaft, which is subject to maximum friction (red dot) and minimum friction (blue dot). Thus a differential heating and a hot spot occurs.

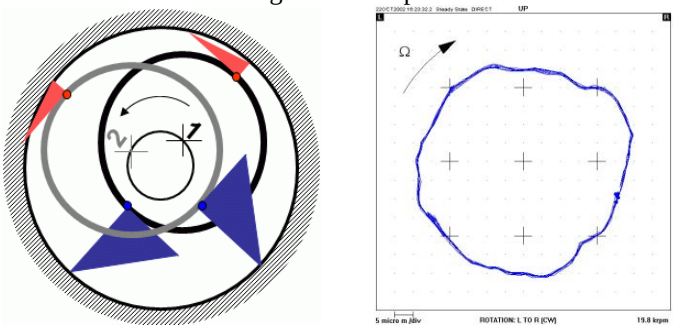

Figure 8. Hot spot mechanism in the bearing and the real circular orbit as tested

For the present case of tilting pad bearings with very low load the case of a centered circular orbit is close to reality as shown in Fig. 8. The estimation of the ratio of added to eliminated heat according to appendix B is among others based on this assumption.

In case of an elliptic off-centered orbit differential heating will also occur. It may be less since it is not always the same two opposite points, which are subject to maximum and minimum friction. On the other side the maximum friction can be higher, since the minimum clearance can be lower. Balbahadur and Kirk [8] claim, that the centered circular orbit is the worst case. However, there is no real evidence from practical experience for this, since hot spot induced spiral vibrations have also been observed in case of highly loaded bearings with elliptic off-centered journal orbits.

The thermal deflection of the shaft due to 1°C temperature difference in the cross section at the bearing on the compressor side is shown in Fig. 9.

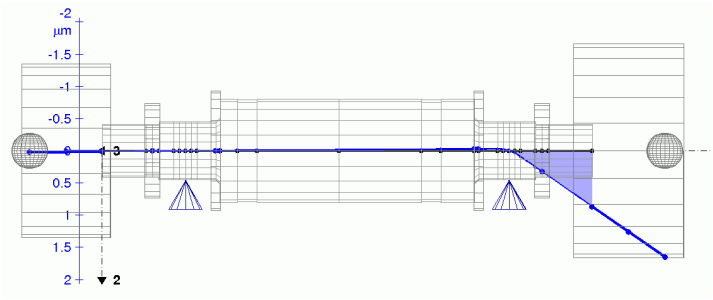

Figure 9. Thermal deformation due to 1°C temperature difference in the compressor bearing

Hot spot stability chart (original design)

The hot spot stability chart for the original configuration is shown in Fig. 10. Hot spots in both bearings were considered in the analysis, which work together and excite the rotor. Therefore two thermal modes (see appendix A) appear. They represent the response to the thermally bent rotor. The threshold of the 1st thermal mode (black line) is determined by the 1st bending and has its minimum at its critical speed. The threshold of the 2nd mode (green line) is determined by the 2nd bending. It is not important in the speed range of interest.

The estimated heat ratio (see appendix B) is the red curve in the chart. It is the ratio of the differential heat generated in the bearing due to losses (which is assumed to enter the shaft) to the differential heat eliminated from the shaft by heat transfer to the oil. Due to the simplifying assumptions, which do not consider the detailed bearing geometry such as the bearing preload and the gaps between the pads, a second heat ratio line (dotted) is drawn assuming only 50% of the input according to Eq. (22) in appendix B. The stability threshold is between the ratio with 100% and 50% heat input. The present and many other experiences prove that in this case there is a large risk to run into a hot spot problem, i.e. to get a spiral vibration with increasing amplitude.

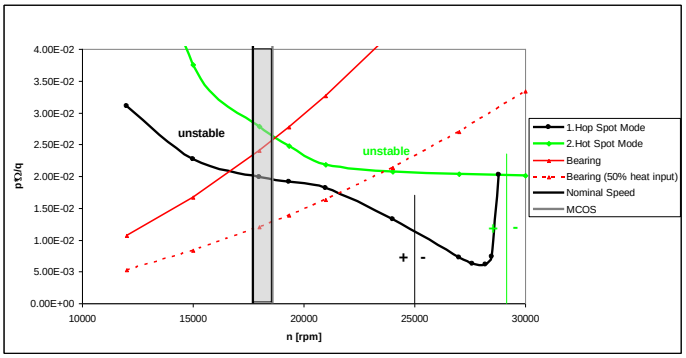

Figure 10. Hot spot stability chart for the original configuration

The direction of the hot spot precession is also indicated in the chart. "+" means the hot spot and thus the phase angle change in the polar plot move in the same direction as the rotor speed, "-" means in the other direction. In the speed range of interest the direction is "+", which agrees with the measurement in Fig. 6.

ANALYZED AND TESTED MODIFICATIONS

Based on the hot spot stability analysis the following three remedies were considered for the elimination of the hot spot phenomena:

- Install modified rotor with higher stiffness
- Reduce the heat input into the shaft in the bearing area
- Increase the heat elimination in the bearing area

Within the existing bearing carrier the rotor can be modified into stiffer execution by elimination of the replaceable thrust collars and by increasing the diameter of the central section.

The reduction of the heat input into the shaft can be accomplished by reduction of the tilting pad bearing to shaft contact area, by reduction of the oil viscosity, or by increasing the bearing clearance.

The heat elimination rate can be increased by higher lube oil flow, or by bearing modifications. The bearing modification can include asymmetric tilting pads, cooling groove in the pads, or pads made of material with higher conductivity e.g. bronze.

In view of the delivery constrains of tilting pads made of bronze the following two configurations have been selected for further testing:

1. modified stiffer rotor
2. bearings with reduced pad width and in addition utilizing lower oil viscosity.

The influence of the bearing parameter changes on the ratio of added to eliminated heat can be seen in Eq. (22) in appendix B. The influence of the lower viscosity is obvious, since the ratio is proportional to it. The influence of a reduced bearing width cannot be directly seen, since it does not appear in the equation. However, the parameter β (thermal deflection per temperature difference in the bearing cross section) is roughly proportional to the width. Thus the ratio is also proportional to the width.

The increase of the bearings clearance was not considered, because it did not bring any significant spiral vibration reduction during the already performed foregoing testing, in spite of the fact that the heat ratio is a square function of the clearance. Most probably the lower heat ratio was compensated by a lower threshold due to a reduction of the 1st bending mode frequency and a larger vibration deflection in the bearing.

The above described modifications 1 and 2 were implemented and internal testing performed to confirm the theoretical results.

Modified stiffer rotor

The original rotor was equipped with replaceable thrust collars. The modified rotor was without replaceable thrust collars and its diameter was increased in the central part. The original and modified rotors are shown in Fig. 11 and 12.

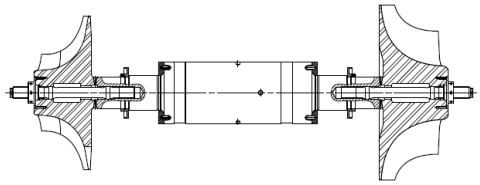

Figure 11. Original rotor

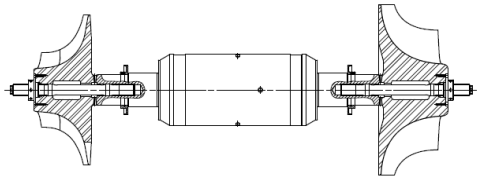

Figure 12. Modified rotor

The Campbell diagram for the 1st forward whirling bending mode of the original and stiffened rotor is shown in Fig. 13. As expected the stiffer rotor increases the separation margin. The damping is reduced. However, due to the large separation margin this should not deteriorate the rotor dynamic performance.

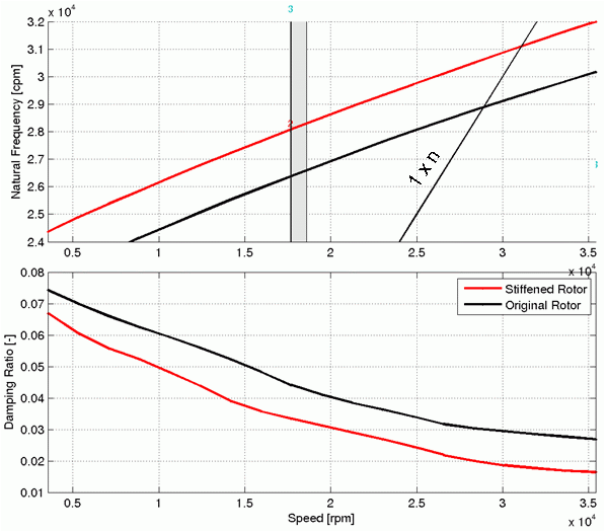

Figure 13. Campbell diagram for the 1st forward whirling bending mode

Hot spot stability chart for the modified rotor

The stability chart of the stiffened rotor is shown in Fig. 14 together with the stability threshold line of the original rotor as dashed lines. The slight improvement of the threshold can be attributed to the higher critical speed, which moves the minimum threshold to a higher speed.

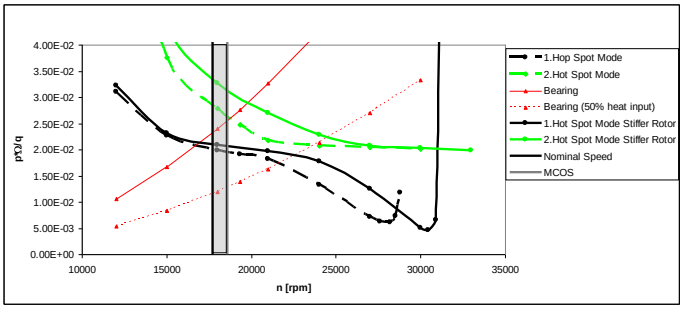

Figure 14. Hot spot stability chart for the modified rotor

Test bed measurements for the modified rotor

The ADRE vibration records for the modified rotor are shown below in Fig. 15-17. It can be seen, that the vibration on the expander side was behaving exceptionally well without any reservations. However on the compressor side, a slight thermal bow by hot spot and spiral vibration was identified in the Bode plot, which shows the vibration hysteresis above the MCOS.

The vibration levels for the modified rotor could be accepted according to the API 617 criteria. But because of the eliminated thrust collars and the beginning hot spot phenomena on the compressor side above the MCOS, this variant was not considered as an acceptable solution.

From this behavior can be concluded, that the actual heat ratio at MCOS is close to the threshold in Fig. 14, i.e. it corresponds to about 80% heat input according to the estimation in appendix B (Eq. (22)).

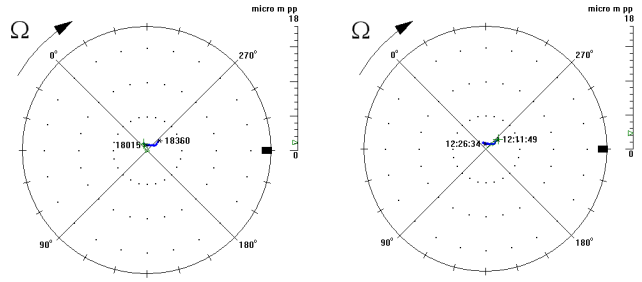

Figure 15. Vibration in polar plot – expander side

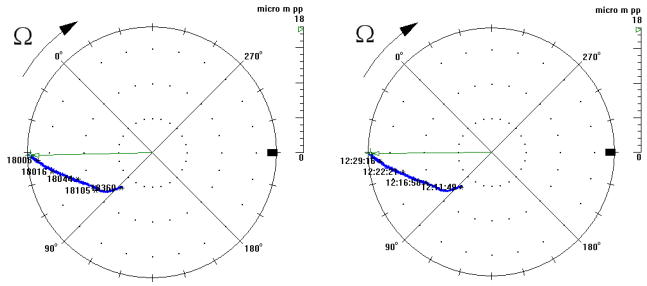

Figure 16. Spiral vibration in polar plot – compressor side

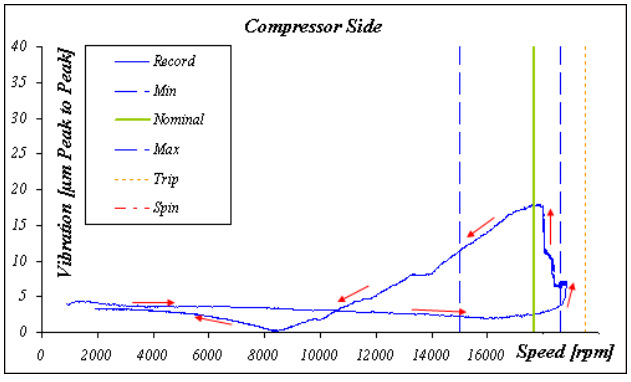

Figure 17. Vibration hysteresis in Bode plot – compressor side

Modified bearings

The original tilting pad radial bearings were of a robust design with a standard width of 0.6D. The contact area to the shaft can be reduced by shortening the pad, by narrowing the bearing width, or by combination of both measures. It was decided to narrow the bearing width from 55 to 40 mm, also in view of the very low bearing loads. The existing original tilting pads and the bearing body were modified as shown in Fig. 18.

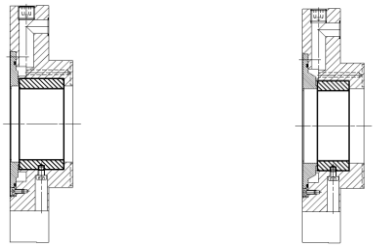

Figure 18. Original 0.6D bearing and modified 0.4D bearing

In addition to the bearing width reduction also the oil viscosity was reduced from nominal 46 cSt to 32 cSt oil. The rotor dynamics was recalculated for the thinner oil and found to be adequate. There was almost no change except a slightly reduced damping.

The two measures reduce the heat input into the shaft approximately by the following factor:

- 40/55 x 32/46 = 0.50

This means that both modifications reduced theoretically the heat input into the shaft to some 50% of the original value. It was important to confirm this assumption by hot spot stability calculation and chart and by testing the new configuration.

Hot spot stability charts for modified bearings with reduced oil viscosity

The stability chart with the bearings with reduced width and the lower viscosity is shown in Fig. 19. The reduced bearing width practically did not change the threshold line, but the heat ratio now is considerably lower. The heat ratio line for 100% heat input is clearly below the threshold in the speed range of interest. Therefore a stable system can be expected.

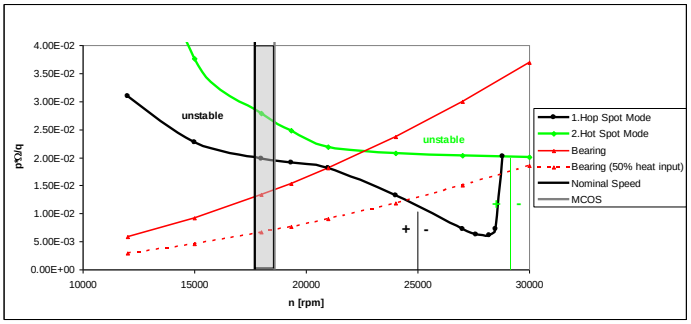

Figure 19. Hot spot stability chart for the reduced bearing width with reduced oil viscosity

Test bed measurements for modified bearings with reduced oil viscosity

With the modified bearings and the oil viscosity reduced from nominal 46 cSt to 32 cSt the test results did not show any more the spiral vibration and vibration hysteresis. With the two described measures the shaft thermal bow due to the hot spot phenomenon and the spiral vibration were completely eliminated up to the tested speed of 22'000 rpm. The test results are shown in Fig. 20 and 21.

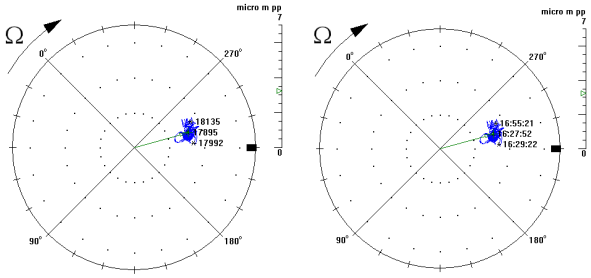

Figure 20a. Vibration in polar plot – expander side

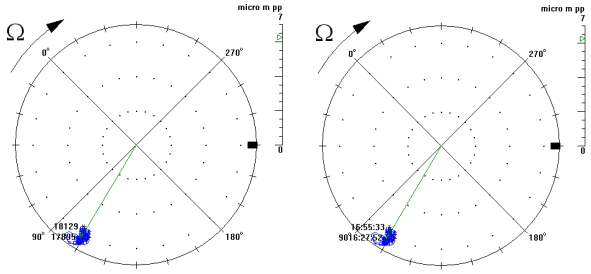

Figure 20b. Vibration in polar plot – compressor side

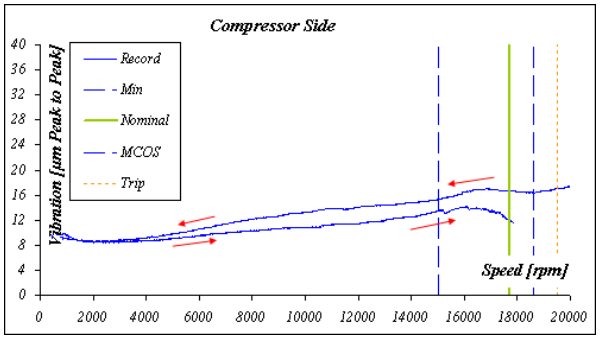

Figure 21. Vibration hysteresis in Bode plot

Decided final configuration

The final configuration of the turboexpander rotor and bearings was decided after the internal testing to be the execution with reduced bearings width and with the reduced lube oil viscosity. With this execution both turbo-expanders and their spare plug-in units were successfully FAT tested with the customer and all accepted without reservations.

EXPERIENCE WITH OTHER TURBO-EXPANDERS

After this new exhaustive experience with the vibration induced hot spots, based on predictive analysis and testing, the unexplained historical cases from the years 1996 and 2001 were analyzed and the unexpected excessive vibrations during FAT were re-evaluated. Both cases with still available ADRE vibration records could be clearly identified as the spiral vibration problem (see Fig. 22 and 23).

Both cases happened on turbo-expanders with similar shaft-bearings configurations as shown in Fig. 2 and 11. The first case (Fig. 22) was identified by slight labyrinth rubbing marks on shaft and was corrected by increasing the labyrinth clearance. The second case was tested up to 104 m/s bearing journal

velocity (Fig. 23) and was corrected during FAT by modification of the bearing clearance. But the vibration problem solving was a kind of a try and error solution, the predictive analytical method was missing.

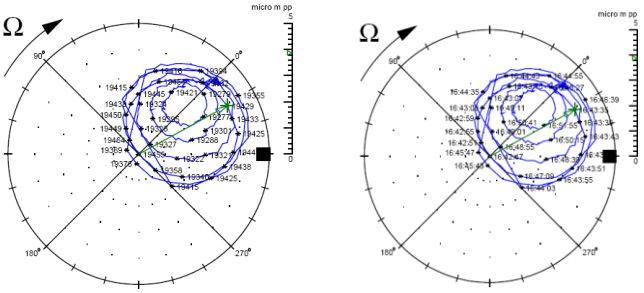

Figure 22. Vibration in polar plot for a case in 1996

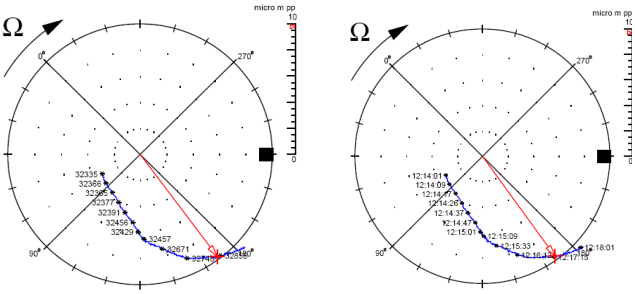

Figure 23. Vibration in polar plot for a case in 2001

In another case of integral gear expander-compressor machine, the predictive hot spot stability analysis was performed during the design stage to eliminate any possible vibration problems in advance. The analysis identified the possible vibration induced hot spot problem and therefore the bearing-shaft configuration was correspondingly and adequately adjusted to improve the heat elimination in the bearing area. During the FAT and also during full load operational test no vibration problems were identified.

CONCLUSIONS

For high speed rotors, even with favorable rotor dynamics evaluation according to the API rules, the hot spot stability analysis as described in this paper is a proven method to determine possible unpredicted vibration problems. As a rule of thumb, all stiff rotors running below the bending critical speed with a journal bearing peripheral velocity above 80 m/s are prone to vibration induced hot spots. For more flexible rotors this threshold speed can be even lower. In this case overhang modes instead of the bending modes influence the appearance of the stability chart. Typically the threshold in the overcritical range then is very low in contrast to the present case, where this is the case in the subcritical range of the 1st bending mode. The reason for this is the location of the vibration node, which is outside the bearing here and inside the bearing in a typical overhang mode.

The vibration induced hot spot behavior in bearings depends on the shaft geometry, the bearing design, the bearing clearance, the lube oil properties (viscosity) and can be influenced by the same. The described advanced hot spot stability analysis can be utilized as the analytic tool to eliminate unforeseen and possible vibration problems already during the design stage. This way the time consuming vibration trouble shooting during the internal testing, the FAT and the start up of high speed rotating machines can be avoided.

The turbo-expanders as described in this paper are today successfully operating in the foreseen speed and load range.

ACKNOWLEDGEMENTS

The authors thank Cryostar SAS for allowing publication of this document.

REFERENCES

[1] Newkirk, B. L., 1926, “Shaft Rubbing. Relative Freedom of Rotor Shafts from sensitiveness to rubbing Contact When Running Above Their Critical Speeds,” Mech. Eng. (Am. Soc. Mech. Eng.), 48(8), pp. 830-832.

[2] Dimarogonas, A. D., 1973, “Newkirk Effect, Thermally Induced Dynamic Instability of High Speed Rotors,” *Proc. ASME Int. Gas Turbine Conference*, Washington D.C., ASME 73-GT-26.

[3] Kellenberger, W., 1978, ”Das Streifen einer rotierenden Welle an einem federnden Hindernis – Spiralschwingungen,“ Ing.-Archiv, 47, pp. 223-229.

[4] Kellenberger, W., 1980 “Spiral Vibrations Due to the Seal Rings in Turbogenerators Thermally Induced Interaction Between Rotor and Stator,” ASME J. Mech. Des., 102, pp 177-184.

[5] Schmied, J., 1987, “Spiral Vibrations of Rotors,” *Proc. 11th Biennal ASME Design Engineering Div. Conference, Vibration and Noise, DE-Vol. 2, Rotating Machinery Dynamics*, Boston MA, ASME H0400B, pp. 449-456.

[6] De Jongh, F. M., and Morton, P. G., 1996, “The Synchronous Instability of a Compressor Rotor due to Bearing Journal Differential Heating,” ASME J. Eng. Gas Turbines Power, **118**, pp. 816-824.

[7] Keogh, P. S., and Morton, P. G., 1993, “Journal Bearing Differential Heating Evaluation With Influence on Rotor Dynamic Behaviour,” Proc. R. Soc. London, Ser. A **441**, pp. 527-548.

[8] Balbahadur, A. C., and Kirk R. G., 2004, “Part I—Theoretical Model for a Synchronous. Thermal Instability Operating in Overhung Rotors,” Int. J. Rotating Machinery, **10**(6), pp. 469–475.

[9] Carrick, H. B., 1999, “Integrally Geared Compressors and Expanders in the Process Industry,” *Proc. Seventh European Congress on Fluid Machinery for the Oil, Petrochemical and Related Industries*, The Hague, IMechE.

[10] Schmied, J., 2007, “MADYN 2000 Documentation,” Delta JS, Zurich.

[11] API 617, 2002, “Axial and Centrifugal Compressors and Expander-compressors for Petroleum, Chemical and Gas Industry Services,” 7th ed., API American Petroleum Institute.

[12] Eckert, L., and Schmied J., 2008, “Spiral Vibration of a Turbogenerator Set: Case History, Stability Analysis, Measurements and Operational Experience,” ASME J. Eng. Gas Turbines and Power, **130**, 012509 (10 pages).

[13] Klement, H. D., 1997, “MADYN Program System for Machine Dynamics, Version 4.2,” Ingenieurbüro Klement, Darmstadt.

NOMENCLATURE

c	Specific heat capacity
f	Vector of external excitation forces
m	Mass of the bearing journal
p	Factor for added heat
q	Factor for eliminated heat
t	Time
u	Bearing peripheral speed
x	Translational deflection coordinate
x	Vector of coordinates
x_T	Thermal translational deflection coordinate
$\mathbf{x}_T$	Vector of coordinates describing the thermal deflection
A	Area of the bearing journal surface surrounded by oil
D	Damping matrix
G	Gyroscopic matrix
K	Stiffness matrix
$\mathbf{K}^R$	Stiffness matrix of the free rotor
M	Mass matrix
P	Bearing power loss
T	Transformation matrix
$\dot{\mathbf{Q}}$	Heating efficiency
α	Real part of the eigenvalue Heat transfer coefficient
β	Relation between thermal deflection and cross sectional temperature difference
δ	Radial bearing clearance
κ	Factor for heat dissipation
λ	Eigenvalue
ν	Imaginary part of the eigenvalue
η	Oil viscosity
K	Factor for heat input
Θ	Cross sectional temperature difference
Ω	Rotor speed in [rad/s]

APPENDIX A

CALCULATION METHOD FOR THE HOT SPOT STABILITY

The equation of motion of the Finite Element model of a multi bearing rotor has the form

$$\mathbf{M}\ddot{\mathbf{x}} + (\mathbf{D}+\mathbf{G})\dot{\mathbf{x}} + \mathbf{K}\mathbf{x} = \mathbf{f}(t) \qquad (1)$$

with the mass matrix **M**, the damping matrix **D**, the gyroscopic matrix **G** and the stiffness matrix **K**. The matrices **D** and **K** are non-symmetric due to the damping and stiffness coefficients of the journal bearings and dependant on rotor speed.

If the rotor is thermally deformed the equation of motion for coordinates **x** relative to the static position of the undeformed rotor is

$$\mathbf{M}\ddot{\mathbf{x}} + (\mathbf{D}+\mathbf{G})\dot{\mathbf{x}} + \mathbf{K}\mathbf{x} - \mathbf{K}^{\mathbf{R}}\mathbf{x}_{\mathbf{T}} = \mathbf{f}(t) \qquad (2)$$

where $\mathbf{K}^{\mathbf{R}}$ is the stiffness matrix of the rotor alone (without pedestals and journal bearings) and $\mathbf{x}_{\mathbf{T}}$ is the vector describing the thermal deformation. The thermal deformation $\mathbf{x}_{\mathbf{T}}$ is assumed to depend linearly on the thermal deflections $\mathbf{x}_{\mathbf{T,HS}}$ of the shaft at a reference location. Typically it is the location of the hot spot (HS).

$$\mathbf{x}_{\mathbf{T}} = \mathbf{T}\,\mathbf{x}_{\mathbf{T,HS}}\,, \qquad (3)$$

$$\mathbf{x}_{\mathbf{T,HS}} = \left(x_{T,h},\, x_{T,v}\right)^{\mathbf{T}} \qquad (4)$$

where $\mathbf{x}_{\mathbf{T,h}}$ and $\mathbf{x}_{\mathbf{T,v}}$ are the thermal translational deflections in horizontal and vertical direction at the location of the hot spot. The matrix **T** is derived from the thermal deformation of the rotor (see Fig. 9), which is determined by a static calculation with thermal loads: for the first column of **T** for a temperature gradient in horizontal direction and for the second column for a temperature gradient in vertical direction.

The modeling of the hot spot phenomenon according to the theory of Kellenberger is based on the following thermal equation:

$$\dot{\tilde{\mathbf{x}}}_{\mathbf{T,HS}} = \underbrace{p\Omega\,\tilde{\mathbf{x}}_{\mathbf{HS}}}_{\dot{\mathbf{Q}}^{+}} - \underbrace{q\,\tilde{\mathbf{x}}_{\mathbf{T,HS}}}_{\dot{\mathbf{Q}}^{-}} \qquad (5)$$

with $\tilde{\mathbf{x}}_{\mathbf{T,HS}}$ as the thermal deflection at the location of a hot spot and $\tilde{\mathbf{x}}_{\mathbf{HS}} = \left(\tilde{x}_h,\, \tilde{x}_v\right)^{\mathbf{T}}$ as the vector of the translational shaft displacements at the location of the hot spot. $\dot{\mathbf{Q}}^{+}$ is the added heating efficiency and $\dot{\mathbf{Q}}^{-}$ is the dissipated heating efficiency.

Equation (5) was derived in detail by Kellenberger (see [3]). The coordinates in Eq. (5) are rotating in contrast to the coordinates in Eqs. (1), (2) and (3) which are stationary.

Equation (5) implies the following:

- The change of cross sectional temperature difference is proportional to the change of thermal deflection,
- the differential heat input across the shaft cross section is proportional to the shaft displacement and the speed,
- the differential dissipated heat across the shaft cross section is proportional to the thermal deflection.

The proportionality factors for the added and dissipated heat are *p* and *q*. Kellenberger has applied the method to simplified shaft models. The method was extended for the use on general shaft systems (see [5]).

Transforming Eq. (5) into stationary coordinates $x_{T,h}$, $x_{T,v}$, x_h, x_v yields

$$\begin{bmatrix} 1 & 0 \\ 0 & 1 \end{bmatrix}\begin{bmatrix} \dot{x}_{T,h} \\ \dot{x}_{T,v} \end{bmatrix}+\begin{bmatrix} -p\Omega & 0 \\ 0 & -p\Omega \end{bmatrix}\begin{bmatrix} x_h \\ x_v \end{bmatrix}+ \begin{bmatrix} q & \Omega \\ -\Omega & q \end{bmatrix}\begin{bmatrix} x_{T,h} \\ x_{T,v} \end{bmatrix}=\begin{bmatrix} 0 \\ 0 \end{bmatrix}, \quad (6)$$

or by using matrices and vectors

$$\mathbf{I}\,\ddot{\mathbf{x}}_{\mathbf{T,HS}}+\mathbf{P}\,\mathbf{x}_{\mathbf{HS}}+\mathbf{Q}\,\mathbf{x}_{\mathbf{T,HS}}=\mathbf{0}. \quad (7)$$

Substituting (3) into (2) and extending (2) by (7) yields

$$\underbrace{\begin{bmatrix} \mathbf{M} & \mathbf{0} \\ \mathbf{0} & \mathbf{0} \end{bmatrix}}_{\mathbf{A}}\begin{bmatrix} \ddot{\mathbf{x}} \\ \ddot{\mathbf{x}}_{\mathbf{T,HS}} \end{bmatrix}+\underbrace{\begin{bmatrix} \mathbf{(D+G)} & \mathbf{0} \\ \mathbf{0} & \mathbf{I} \end{bmatrix}}_{\mathbf{B}}\begin{bmatrix} \dot{\mathbf{x}} \\ \dot{\mathbf{x}}_{\mathbf{T,HS}} \end{bmatrix}+ \underbrace{\begin{bmatrix} \mathbf{K} & -\mathbf{K}^{\mathbf{R}}\mathbf{T} \\ \mathbf{P} & \mathbf{Q} \end{bmatrix}}_{\mathbf{C}}\begin{bmatrix} \mathbf{x} \\ \mathbf{x}_{\mathbf{T,HS}} \end{bmatrix}=\begin{bmatrix} \mathbf{0} \\ \mathbf{0} \end{bmatrix} \quad (8)$$

where **P** is a 2 x *N* matrix (with *N* as the dimension of Eq. (2)), which has the coefficients of **P** at the columns of the translational coordinates $\mathbf{x}_{\mathbf{HS}}$ of the hot spot.

To receive Eq. (8) the original Finite Element model of the rotor represented by Eq. (1) must be extended by introducing the two extra degrees of freedom $x_{T,h}$ and $x_{T,v}$. The additional coefficients must be added to the global matrices. This possibility is provided for the input of the program MADYN [13].

From Eq. (8) one could calculate the time history of **x** by a time step method. The polar plot of the time history of each coordinate would be a spiral either increasing or decreasing in magnitude. This calculation however would require larger computational effort, since the period of a spiral to complete a 360°-turn is very long for realistic examples. That is why the computation would require the simulation of quite a long period of time until one could judge whether a spiral increases or decreases in magnitude.

As described in [5] this information can be easier extracted from the complex eigenvalues of Eq. (8). Their calculation requires little computational effort.

Equation (8) has 2(N+1) eigenvalues. Since realistic values for *p* and *q* are very small a set of 2N eigenvalues are practically the same as those of Eq. (1) representing the rotor system.

The additional two eigenvalues are a conjugate complex pair

$$\lambda_T = \alpha \pm i\nu. \quad (9)$$

They will be called „thermal“ eigenvalue in the following. The imaginary part ν of the thermal eigenvalue is almost equal to Ω. The interpretation of the thermal eigenvector (so-called hot spot mode) is derived in [5]:

The difference between ν and Ω indicates how fast the thermal bow moves along the shaft respectively at which speed the spiral is traced. The period to complete 360°-turn of the spiral is

$$T = 2\pi / |\nu - \Omega|. \quad (10)$$

The direction of the revolution of the unbalance response vector is as follows:

$\nu > \Omega$, forward (co-rotational, same direction as the rotor spin)

$\nu < \Omega$, backward (counter- rotational, opposite direction as the rotor spin).

The real part of the thermal eigenvalue λ_T indicates whether the spiral increases or decreases in magnitude:

$\alpha > 0$, increasing magnitude (unstable behavior)

$\alpha < 0$, decreasing magnitude (stable behavior).

To receive the stability threshold the heat input (i.e. the factor p) is varied until the real part becomes $\alpha = 0$.

The method can also be applied for more than one hot spot by extending Eq. (8) accordingly. The number of additional “thermal” eigenvalue pairs corresponds to the number of hot spots.

APPENDIX B

ESTIMATION OF THE RATIO OF ADDED TO ELIMINATED HEAT FOR A FLUID FILM BEARING

The ratio of the added to eliminate heat is estimated with the help of the following simplifying assumptions:

1. The journal orbit is a synchronous circle.
2. The radial clearance around the circumference is constant.
3. The circumferential distribution of the added heat due to the vibration is a sinus shape. The maximum is at the high spot of the shaft.
4. For the eliminated heat distribution the same applies as for the added heat.
5. The axial distribution of the temperature in the journal is constant.
6. The journal ends are adiabatic.
7. The complete sinus shaped friction power due to the vibration enters the shaft (not the oil).

These assumptions are best fulfilled for an unloaded cylindrical bearing.

The thermal equation for the cross sectional temperature difference Θ in the journal is:

$$\dot{\Theta} + \kappa\Theta = \mathrm{K} \tag{11}$$

with

$$\kappa = \frac{3\alpha A}{mc}, \tag{12}$$

$$\mathrm{K} = \frac{3\pi}{2mc}\Delta\dot{Q} \tag{13}$$

and m as the mass of the journal, c as the specific heat capacity, A as the surface area of the journal surrounded by oil, α as the heat transfer coefficient and $\Delta\dot{Q}$ as the added heat.

The thermal equation according to Kellenberger has the following form (also see A5):

$$\dot{x}_T = p\Omega x - q x_T \tag{14}$$

with x as the radius of the circular journal orbit and x_T as the thermal deflection.

The relation between x_T and θ is:

$$x_T = \beta\Theta, \tag{15}$$

where β has to be determined from the rotor model by assuming a temperature difference across the journal. For the thermal deflection any reference location on the rotor could be taken. The ratio of added to eliminated heat depends on this location, but the stability threshold will adjust accordingly. Typically the location at the hot spot is taken (also see Eq. (3)).

(15) substituted into (14) yields:

$$\dot{\Theta} + q\Theta = \frac{p\Omega}{\beta} x. \tag{16}$$

Comparing (16) and (11) considering (12) and (13) yield:

$$q = \frac{3\alpha A}{mc}, \tag{17}$$

$$\frac{p\Omega}{\beta} x = \frac{3\pi}{2mc}\Delta\dot{Q}. \tag{18}$$

(17) and (18) yield:

$$\frac{p\Omega}{q} = \frac{\pi\Delta\dot{Q}\beta}{2x\alpha A}. \tag{19}$$

The added heat can be estimated as

$$\Delta\dot{Q} = \frac{2}{\pi} P \frac{x}{\delta} \tag{20}$$

with the bearing power loss P

$$P \approx \frac{u^2\eta A}{\delta}, \tag{21}$$

the viscosity η, the peripheral speed u and the radial bearing clearance δ.

(20) and (21) substituted into (19) yields:

$$\frac{p\Omega}{q} = \frac{u^2\eta\beta}{\delta^2\alpha}. \tag{22}$$